Journal of Magnetic Resonance 307 (2019) 106587

Contents lists available at ScienceDirect

Journal of Magnetic Resonance

journal homepage: www.elsevier.com/locate/jmr

Modulation sidebands spectra within inhomogeneous CW-EPR line detected by double modulation EPR spectroscopy

B. Rakvin *, D. Carić, M. Kveder

Ruđer Bošković Institute, Division of Physical Chemistry, Bijenička 54, Zagreb, Croatia

ARTICLE INFO

Article history:
Received 15 July 2019
Revised 26 August 2019
Accepted 28 August 2019
Available online 30 August 2019

Keywords:
EPR
Magnetic field modulation
Double magnetic field modulation
Modulation sidebands
E'-centers in quartz

ABSTRACT

Conventional modulation spectrum, MS, in continuous wave electron paramagnetic resonance, CW-EPR, is produced by applying longitudinal radiofrequency (RF) fields with the frequencies, ω_{rf}, which exceeds the linewidth, $2\pi\delta$, of a single spectral line given in frequency units. The second longitudinal RF field with frequency, ω_{rf2}, is employed to produce double modulation spectrum, DMS. In this work DMS are presented as a specific type of MS which can be produced from an ordinary homogenous line. The numerical simulations of DMS in the limit of low power saturation relied on the recently introduced multi-photon transitions formalism which includes one microwave photon in combination with an arbitrary number of radiofrequency photons. It is shown that DMS of an inhomogeneous line exhibits similar basic structure as MS and exhibits sideband peaks at multiples of basic radiofrequencies. Linewidths of these peaks are significantly narrower (cca. two – three orders of magnitude) than the inhomogeneous linewidth and can be correlated with the underlying homogeneous linewidth components on the basis of characteristic spin-lattice, T_1, and spin-spin, T_2, relaxation times. The capability to extract T_1 and T_2 from DMS was tested on the well-known E' defect in irradiated vitreous SiO_2. The obtained results revealed the impact of "rapid passage" effect on DMS in improving the detection sensitivity of DMS in the study of paramagnetic centers with long relaxation times. Therefore, double modulation method can be considered as a complementary method for studying inhomegeneous broadening in the EPR spectra.

1. Introduction

In recent years' studies of spin systems containing very long relaxation times (transverse, T_2 and longitudinal, T_1) started to be of interest due to their potential application in quantum information technologies. The capability to extract narrow homogeneous line (spin packet) from the Pulsed-EPR data, has been used to deduce T_1 and T_2 of the monitored spin system. Interestingly, several decades ago it was suggested that the CW-EPR method based on modulation sidebands, MS, known as Double Modulation EPR, DM-EPR, can be also used as a method complementary to the Pulsed-EPR in detection of a very narrow "spin packet-like" line from an inhomogeneous line [1–7]. Early theoretical studies of MS and DM-EPR spectra, DMS, were mostly based on semi-classical approach [1,8] by applying modified Bloch equations [9] or nonlinear radio-frequency absorption formalism [10]. All these theoretical models only partially described the properties of DMS. Overall, they predicted well only the appearance of the peaks in the frequency scale but they failed to describe different lineshapes as well as saturation effects at a higher microwave, MW, field in DMS.

However, modulation effects in CW-EPR spectroscopy were recently revisited and explained by introducing multi-photon transitions [11–13]. By using quantized radiation fields, it was shown that MS, when the modulation frequency, ω_{rf}, exceeds the line width, $2\pi\delta$, can be described by the multi-photon transitions. In this formalism one MW, σ^+ photon is absorbed from the MW radiation field and an arbitrary number k of radiofrequency, RF, π photons are absorbed from or emitted to the modulation RF field ($\sigma^+ + k \times \pi$). In such general approach one of the most often cited model, convenient for the EPR case, addresses the resonant interaction between these bichromatic fields [14] i.e. transverse MW field, B_{mw}, and longitudinal RF field, B_{rf}, while the two level spin system (spin qubit) is experiencing the Zeeman magnetic field, B_0. Therefore, the effective magnetic field acting on the observed spin system is:

$$B = B_0 + B_{rf} + B_{mw} \quad (1)$$

with the components in the laboratory frame of reference $B_z = B_0 + (2\omega_2/\gamma)\cos(\omega_{rf}t)$ and $B_x = (2\omega_1/\gamma)\cos(\omega_{mw}t)$ while γ is

* Corresponding author at: Institute Ruđer Bošković, Bijenička 54, 10000 Zagreb, Croatia.
E-mail address: rakvin@irb.hr (B. Rakvin).

https://doi.org/10.1016/j.jmr.2019.106587
1090-7807/

the electron gyromagnetic ratio. Linearly polarized MW field with amplitude ($2\omega_1 = \gamma B_1$) is oriented along the x axis of the laboratory frame of reference while the linearly polarized RF field with amplitude ($2\omega_2 = \gamma B_2$) and static magnetic field giving rise to the Larmor frequency ($\omega_0 = \gamma B_0 = g_e\mu_B B_0/\hbar$) of electron spins are both directed along the z axis.

The calculated spin dynamics can be expressed in terms of frequency parameters ω_2 and ω_1 denoting the amplitudes of RF and MF fields in frequency units, respectively [12]. It is convenient to introduce two different regimes of the spin dynamics in terms of: "weak modulation near the Rabi resonance", WMRR, and "strong and fast modulation", SFM with the corresponding values of the applied RF modulation, $\omega_2 \ll \omega_1 \approx \omega_{rf}$ and $\omega_2 > \omega_1 \ll \omega_{rf}$, respectively. For each of these spin dynamics regimes description of MS spectrum was derived in analytical form and can be used as a starting point for the description of double MS and further numerical simulation of DMS expected in the same regimes.

In the present study numerical simulation of DMS will be presented for the first time by employing newly suggested multi-photon transitions to describe MS and CW-EPR spectra acquired at the low microwave power, P_{mw}, intensity. Under this condition and small ω_2 applied, MS shows specific properties (shift between sidebands lines, and larger dispersion intensity than absorption intensity of MS) which also affects DMS. In the region of high P_{mw} intensity the effect of "rapid passage" in CW-EPR [15,16] on DMS will be detected and discussed. It will be shown that lineshapes and saturation effects in DMS experimentally detected for well-defined standard system with long relaxation times, E' defect in irradiated vitreous SiO_2, can be more accurately interpreted by applying later description.

2. Amplitude modulation in CW-EPR

2.1. Modulation spectrum of homogeneous EPR line

In order to calculate the absorption EPR signal, one can follow the recent description of CW-EPR spectra [12] and use the simple Hamiltonian of a spin qubit (spin S = 1/2) with the ground $|1\rangle$ and excited $|2\rangle$ states exposed to three magnetic fields described by the Eq. (1). The CW-EPR signal is proportional to the transverse component of the steady-state magnetization out-of-phase with the MW field. The most often detected signal in the form of the first-harmonic is given for SFM regime reads [12]

$$\langle S_y\rangle_1 = \sum_{k=-\infty}^{\infty}\left[\frac{T_2\omega_1 J_{-k}(z)[J_{1-k}(z)+J_{-1-k}(z)]}{1+\omega_1^2 J_k^2(z)T_1T_2+\left(\Omega_S-k\omega_{rf}+\Delta_{BS}(k)\right)^2T_2^2}\cos\left(\omega_{rf}t\right) - \frac{\left(\Omega_S-k\omega_{rf}+\Delta_{BS}(k)\right)T_2^2\omega_1 J_{-k}(z)[J_{1-k}(z)-J_{-1-k}(z)]}{1+\omega_1^2 J_k^2(z)T_1T_2+\left(\Omega_S-k\omega_{rf}+\Delta_{BS}(k)\right)^2T_2^2}\sin\left(\omega_{rf}t\right)\right]$$

$$\Delta_{BS}(k) = \frac{1}{2}\sum_{n\neq k}\frac{\omega_1^2}{(k-n)\omega_{rf}}J_n^2(z) \qquad (2)$$

with $\Omega_S = (\omega_0-\omega_{mw})$ denoting the resonance offset and $z = 2\omega_2/\omega_{rf}$ representing the modulation index of Bessel function of the first kind and order k, J_k, while $\Delta_{BS}(k)$ represents the term known as Bloch-Siegert-like shift. Eq. (2), with respect to the RF field, consists of in-phase components exhibiting absorption shapes and out-of-phase components displaying dispersion profiles. Both contributions are anti-symmetric with respect to the center of MS spectrum. It is important to mentioned that classical Bloch equations give the same description for the first-harmonic spectrum [9] as given in (2) but without the saturation term in denominator and the term describing Bloch-Siegert-like shift. The sidebands due to the multi-photon transitions appear with slightly corrected mutual displacement of $\Delta B = (\omega_{rf}-\Delta_{BS})/\gamma$ in the spectrum and their intensity

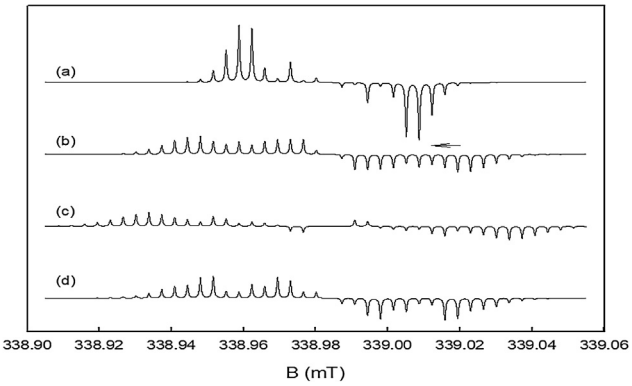

Fig. 1. First-harmonic in-phase sideband spectra for the single homogeneous line calculated by employing Eq. (2): single modulation (a) and Eq. (3): double modulation (b, c, d). Parameters of the homogenous line are: $T_1 = T_2 = 2.0\times10^{-5}$ s, δ = 15.915 kHz); the first modulation frequency, amplitude, and index are: $\omega_{rf}/2\pi$ = 100 kHz, $\omega_2/2\pi$ = 400 kHz, z = 8 and: $\omega_1/2\pi$ = 0.55 kHz are same for the all spectra. The second modulation parameters are: $\omega_{rf2}/2\pi$ = 200 kHz, $\omega_{22}/2\pi$ = 300 kHz, z' = 3 (b); $\omega_{rf2}/2\pi$ = 200 kHz, $\omega_{22}/2\pi$ = 500 kHz, z' = 5 (c); and $\omega_{rf2}/2\pi$ = 300 kHz, $\omega_{22}/2\pi$ = 300 kHz, z' = 2 (d). Resolution for all calculated sidebands spectra is 0.1 μT at magnetic field scale. The arrow points to the most intensive peak in the spectrum (a).

(saturation) depends on $J_k^2(z)$. The Bloch-Siegert-like shift shows k^{-1} dependence and its contribution is important only for the sidebands exhibiting very low k i. e. for the first and the second sidebands near the center of a spectrum. This effect was recently employed to improve the accuracy in evaluation of MW field strength from measurements of the frequency splitting between the first sidebands in MS spectrum [17]. For the multi-photon transitions, with higher $|k|$ value and approximately equal z value the obtained Δ_{BS} is expected to be negligible small. On the other side, for higher values of $|k|$ multi-photon transition gives maximum contribution to the first-harmonic signal [11]. Thus, for example, the standard CW-EPR signal detected at 100 kHz with amplitude modulation of 0.1mT exhibits $z \sim 30$ while the most intense sideband consists of absorption of one σ- and 28 π-photons being positioned at 28th sideband in the spectrum. Assuming homogeneous line is broader than the modulation frequency ($1/T_2 \gg \omega_{rf}$), the Eq. (2) gives for the first derivative lineshape a typical CW-EPR line detected at the first harmonic [11].

2.2. Simulation of DM-EPR spectra

In order to describe DMS it is convenient to use only the part of MS with the largest sideband intensities. At this spectral position only small contribution of Δ_{BS} is expected, thus, it can be dropped out in the further calculation. The second modulation field in terms of $2\omega_{22}\cos(\omega_{rf2}t)$ is introduced as an additional modulation source for each sideband (multi-photon absorption lineshape). Here, the second RF field, RF2, produces additional (the zero-harmonic type) sidebands in the first-harmonic in-phase spectrum. Following previous discussions on the second modulation employed [1,8,10], description of DMS is suggested in the form of double summation:

$$D\langle S_y\rangle_{1in} = \sum_{k'=-\infty}^{\infty}\sum_{k=-\infty}^{\infty}\left[\frac{T_2\omega_1 J_{-k}(z)[J_{1-k}(z)+J_{-1-k}(z)]j_{k'}^2(z')}{1+\omega_1^2 J_k^2(z)j_{k'}^2(z')T_1T_2+\left(\Omega_S-k\omega_{rf}-k'\omega_{rf2}\right)^2T_2^2}\right] \qquad (3)$$

where $z' = 2\omega_{22}/\omega_{rf2}$ is the modulation index of Bessel function of the first kind and order k' related to RF2 field. It is important to note that in the Eq. (3) the saturation term, $\omega_1^2T_1T_2$, depends on both modulation frequencies through the corresponding Bessel functions. Fig. 1 shows typical MS obtained from (2) for chosen param-

eters given in the figure caption. In Fig. 1a the arrow denotes the most intense peak ($k \sim 7$) as is expected for applied $z = 8$ value. It is also important to note that the various intensity of sidebands can be seen in the magnetic field spanning the interval from the center of spectrum to the sideband with the largest intensity. The sidebands outside of this range exhibit an exponential decay at higher magnetic field. By applying the RF2 field according to the Eq. (3) the same spectrum is additionally modulated as shown in Fig. 1b–d. It is clear that the additional modulation, besides exhibiting more complex spectral properties in terms of more lines with various sideband intensities and peaks with opposite orientation within the one of antisymmetric spectral parts (Fig. 1c), does not show any other qualitatively important information about MS. Therefore, in the next step the methodology of DM-EPR will be applied in order to simulate DMS i.e. "sideband peaks" as a function of the second modulation frequency. The peak of D $<S_y>_{1in}$ is expected on the ω_{rf2} scale when the term ($\Delta_{kk'} = \Omega_S - k\omega_{rf} - k'\omega_{rf2}$) in Eq. (3) as function of ω_{rf2} reaches the value of zero,

$$\omega_{rf2} = \frac{\Omega_S}{k'} - \frac{k\omega_{rf}}{k'} \tag{4}$$

In the first step the static magnetic field B_0 is shifted to the position B_{oos} of the peak with the most intense sideband ($k \approx z$) as denoted on Fig. 2a. At this fixed field position the change of D $<S_y>_{1in}$ as a function of ω_{rf2} is calculated (Fig. 2b). The obtained spectrum indeed shows peaks at positions of multiple of the first modulation frequency $k\omega_{rf}$ ($k = 1, 2, 3, \ldots$) as is expected in the standard DMS. (It can be noted that by shifting of the magnetic field to the position corresponding to the top of the 7th sideband peak actual Ω_S reaches the value which is multiple of ω_{rf} and Eq. (4) became multiple of ω_{rf}.) One of these peaks, the peak at $\omega_{rf2}/2\pi = 300$ kHz, is fitted with Lorentzian lineshape (insert to Fig. 2b) providing the corresponding fitted value of $\delta = 15.96$ kHz, which is very close to the linewidth of the un-modulated homogeneous line ($\delta = 15.91$ kHz). This result is qualitatively expected since the intensity of this as well as other peaks consists of sum of neighboring sideband peaks produced by the second modulation field (additional schematic descriptions can be seen in Refs. [8,10]). Moreover, there is an indication of low intensity peaks present at half values of modulation frequencies (visible at 50 kHz and 150 kHz in the spectrum shown in Fig. 2b) as is expected for DMS spectra ($k' > 1$, Eq. (4)). To examine in detail properties of these simulated spectra the gradual change of all parameters within SFM regime is presented in Fig. 3. In specific, an example is shown where all parameters are the same as in Fig. 2 except for T_2 and T_1, which are an order of magnitude larger. Consequently, the linewidths of sidebands are ten times narrower ($\delta = 1.591$ kHz) while their spectral intensity distributions are similar to distributions of sideband exhibiting broader linewidths shown in Fig. 2a. This change is also reflected in the double modulation spectrum in which almost an order of magnitude narrower peaks appears (Fig. 3b). The fitted peak at 300 kHz shows significant change of the linewidth ($\delta = 1.76$ kHz). In the next step only the microwave field strength, $\omega_1/2\pi = 0.55$ kHz, is replaced with the order of magnitude larger value $\omega_1/2\pi = 5.5$ kHz still being within SFM regime, while all the other parameters are kept the same as parameters used in Fig. 3. Here, significant change of

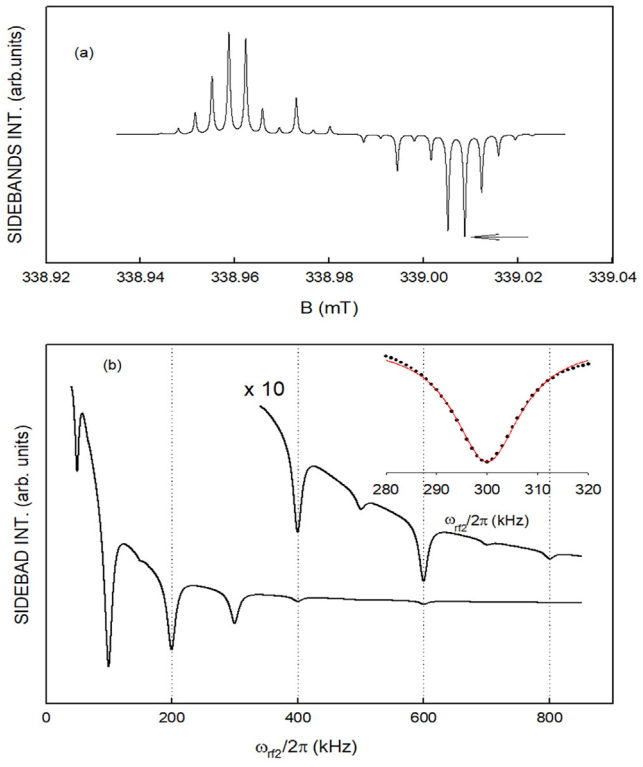

Fig. 2. Sideband (a) and double modulation (b) spectra of a single homogeneous line. The sideband spectrum was calculated by employing Eq. (2) and parameters given in Fig. 1. For double modulation spectrum the magnetic field was fixed at position of 7th sideband peak ($B_{oos} = 339.0158$ mT) as denoted by arrow in (a) and intensity of this peak is evaluated as a function of the second modulation frequency $\omega_{22}/2\pi = 500$ kHz (in steps of 1 kHz) using Eq. (3). The obtained peaks appeared at multiple of the first modulation frequency. Inserts show the fitted Lorentzian lineshape (red line) of the third peak at 300 kHz with $\delta = 15.96$ kHz and enlarged part of the spectrum at higher frequencies. (For interpretation of the references to colour in this figure legend, the reader is referred to the web version of this article.)

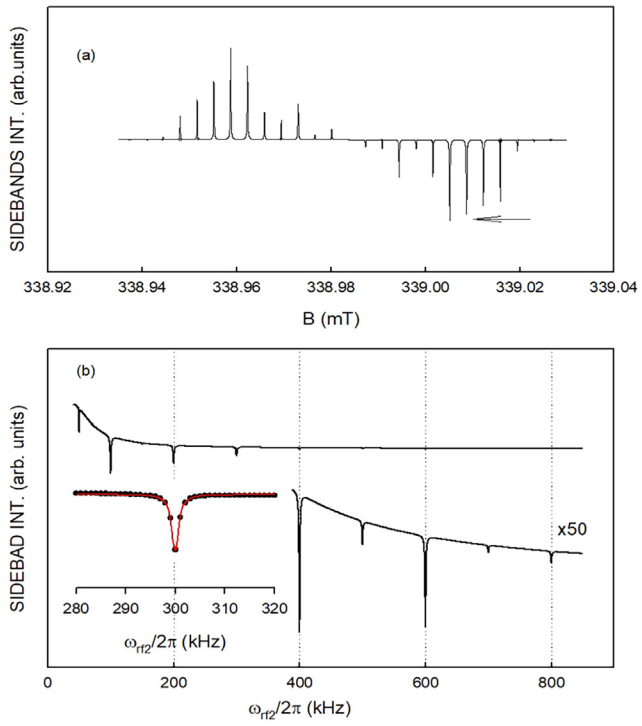

Fig. 3. Sideband (a) and double modulation (b) spectra of a single homogeneous line. Calculation performed with the same spectral parameters as in Fig. 2a and b expect for relaxation times which are replaced for one order of magnitude longer times, narrower linewidth, ($T_1 = T_2 = 2.0 \times 10^{-4}$ s, $\delta = 1.59$ kHz). In (b) the left insert shows fitted Lorentzian lineshape (red line) of the third peak at 300 kHz with $\delta = 1.76$ kHz and the right insert enlarged part of the upper spectrum. (For interpretation of the references to colour in this figure legend, the reader is referred to the web version of this article.)

sideband spectra related to saturation broadening of peaks can be seen (Fig. 4a). This saturation broadening affects broadening of peaks with non-uniform distribution along the spectrum. Peaks in the spectral region from the center of spectrum to the peak with maximum intensity show a linewidth distribution of sidebands. The narrowest sideband lines appear for k higher than k corresponding to the sideband with the maximum intensity. This effect can be easily explained in terms of the saturation factor in Eq. (2), which depends on Bessel function. Thus, the sideband spectrum of homogeneous line under the saturation condition will not exhibit the sideband spectrum with equal linewidths of the sideband peaks. It is also expected that linewidths in the double modulation spectrum will be influenced by the similar effect. Indeed, Fig. 4b indicates that linewidths of the peaks in the low region of the sweeping frequency are generally broader than the less saturated peaks at higher frequencies (peaks with larger multiples, $k\omega_{rf}$). In order to reach more reliable linewidth estimation of the originally homogeneous line from the DMS one can apply large z-value and detect peaks with largest possible $k\omega_{rf}$. The same effect can be used to describe the line positioned at multiple of the half of modulation frequency (for example line at (3/2)100 kHz in Fig. 4b). These types of lines at $(k/k'\omega_{rf})$ generally appear narrower than the neighboring lines at $k\omega_{rf}$ since they consist of lines with higher $k = 3$ than the $k = 1$ and $k = 2$ of neighboring lines. Fig. 4c represents DMS spectrum obtained with the same parameters as shown in Fig. 4b but with different position of B_{oos}. In the present case the B_{oos} is shifted

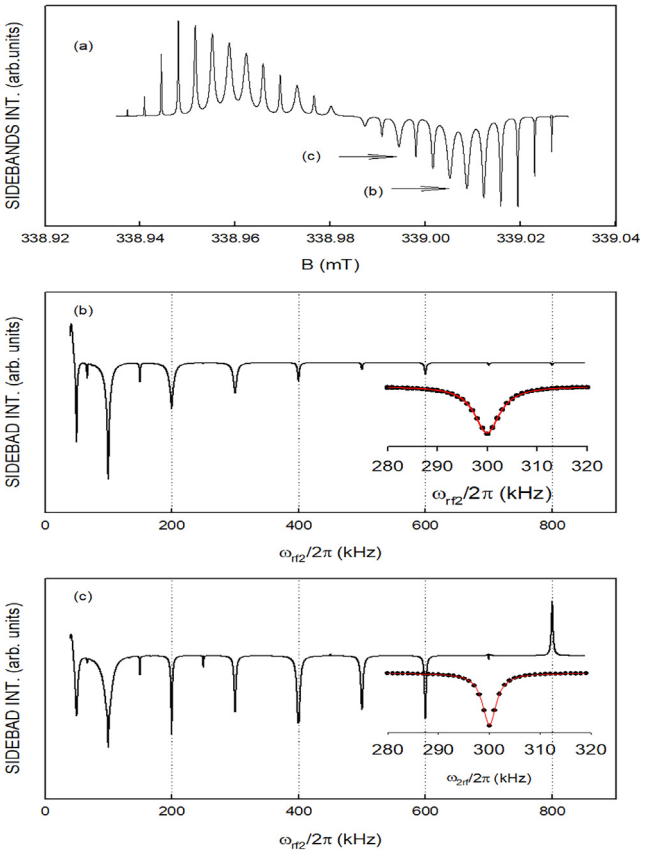

Fig. 4. Sideband (a) and double modulation (b, c) spectra of a single homogeneous line. Calculation performed with the same parameters as in Fig. 3a and b except for the microwave power which was larger by an order of magnitude ($\omega_1/2\pi = 5.5$ kHz) (b) and positioning magnetic field ($B_{oos} = 338.9908$ mT) at different sideband peak (c). The sidebands peaks involved in (b, c) are denoted by arrows in (a). Peaks (at 300 kHz) fitted by Lorentzian lineshapes with $\delta = 6.07$ kHz and $\delta = 3.28$ kHz are shown as inserts in (b) and (c).

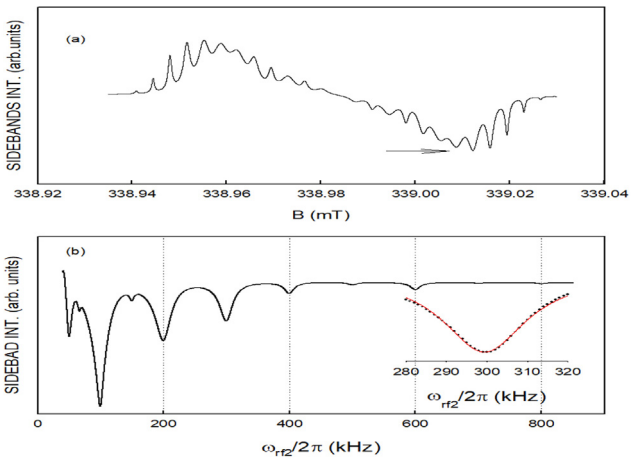

Fig. 5. Sideband (a) and double modulation (b) spectra of a single homogeneous line Calculation performed with the same parameters as in Fig. 4a and b except for the relaxation time which is replaced with an order of magnitude faster value $T_2 = 2 \times 10^{-5}$ s ($\delta = 15.915$ kHz). The insert in (b) shows peak (at 300 kHz) fitted by Lorentzian lineshape with $\delta = 25.12$ kHz.

to lower magnetic field (338.9908 mT) which matches the position of the top of the forth sideband, as denoted by arrow in Fig. 4a. Again, the similar DM-EPR spectra appear with peaks at the same frequencies as those shown in Fig. 4b but exhibiting different intensities. Moreover, peaks at 700 kHz and 800 kHz start to change orientations due to closer positioning of B_{oos} with respect to the center of the spectrum containing contributions of sidebands with positive orientations (Fig. 4a). It can be also noted that the 4th peak appears narrower than the 7th peak with corresponding peaks $\delta = 6.07$ kHz and $\delta = 3.28$ kHz, respectively. The above example shows an additional origin of variations of the linewidths of spectral peaks in the DMS of the homogeneous line. Finally, we address the model which assume significantly different T_2 in comparison to T_1 (Fig. 5). All parameters are kept the same as in Fig. 4b except for smaller value (order of magnitude) used for T_2. Here, a significantly lower resolution in sideband spectrum can be noted (Fig. 5a) with the expected broader linewidth at lower peak position ($\delta = 25.12$ kHz for peak at 300 kHz and $\delta = 18.04$ kHz for peak at 600 kHz) as shown in insert to Fig. 5. It is obvious that upon further decreasing of T_2 value, the structure of DMS peaks will be lost.

2.3. DM-EPR spectrum of inhomogeneous EPR line

As was mentioned above the DM-EPR method was used to detect a narrow i.e. "spin packet-like" spectral lines in an inhomogeneous EPR line. This property of DM-EPR method was discussed in the frame of suggestions proposed in several theoretical models of the method [8,10]. It can be noted that those models lead to different descriptions of phenomena in DM-EPR. This is due to the assignation of different contributions appearing as dominant terms in the calculations. In specific, Giordano et al. considered the case of $T_1 \gg T_2$ and suggested that the linewidths in DMS originated from T_1 relaxation time, while Dulčić and Perić [8] claimed that observed lineshape originated from T_2 and eventually T_1 in the center of the line. Both theoretical models considered DMS only in the limit of small MW power.

Here presented analysis has no intention to go into detailed theoretical simulation and discussion of above phenomena but rather, to provide qualitative description and make the comparison easier with the case of homogeneous line as well as to discuss experimentally detected DMS of an inhomogeneous EPR line. It should be noted that when considering an inhomogeneously broadened

EPR line, besides *dc* field B_0, an additional local field, B_L, is required to be introduced. B_L is variable and corresponds to various spin packets within an inhomogeneous line. The contribution of various spin packets is given by its weight in the inhomogeneous distribution function $g(B_L)$. Thus, in the frequency domain B_L is transformed into the local frequency ω_L and can be easy introduced in above calculations as a newly defined resonance offset, $\Omega_{SL} = \Omega_S + \omega_L$. Various MS centered at Ω_{SL} within an inhomogeneous spectral line can be produced by employing modulation frequency with larger frequency than the linewidth of a spin packet. However, here appears the problem of how to choose the magnetic field at exact position exactly at the top of a sideband peak of the produced MS spectra, similarly as in the case of a homogenous line discussed above. It can be expected that at an arbitrary magnetic field position (usually it is the position exhibiting the large number of multi photon transitions, $k \sim z$) there are certain number of sideband peaks for which Ω_{SL} is multiple of ω_{rf}. Nevertheless, such sideband peaks can be treated as in the case of the homogeneous line. In the process of sweeping the second modulation frequency there are also peaks between various sideband peaks within an inhomogeneous line (k', multiple photon transitions) for which the Eq. (4) is valid. At this resonance condition one expects that the envelope of inhomogeneous line will be affected and DM-EPR peak will be detected [8,10]. Finally, for an arbitrary magnetic field position there are also additional spin packets within the interval of $\pm 1/2\omega_{rf}$, which are somewhat shifted from the spin packets positioned as mentioned above and it is interesting to consider their contribution in DMS. Therefore, in order to better describe the impact of inhomogeneous line on DMS let us consider a simplified model of an inhomogeneous line containing fifteen spin packet lines at the corresponding local magnetic fields and exhibiting the same linewidth (δ = 1.591 kHz). Ten spin packets are symmetrically distributed around the central spin packet with mutual shifts of 10 kHz while four spin packets are symmetrically distributed about the central spin packet with mutual shifts of 2.5 kHz. The intensities of these packets are described using Gaussian profile with linewidth of 83.25 kHz as schematically presented in Fig. 6. The MS is shown for one half of the entire spectrum exhibiting negative intensity contributions (Fig. 7a) and assuming the same modulation condition as in the Fig. 3. The largest intensity of the MS originates from the central spin packet chosen at the position B_{oos} for detection of DMS. During the second modulation frequency sweep the response of each spin packet and corresponding DMS are monitored. DMS of the central sideband (Fig. 7b) shows the same type of DMS as was obtained in Fig. 3. The two spin packets positioned at ±2.5 kHz from the central spin peak lead to two DMS with not equal and shifted peaks shown in Fig. 7b. In addition, DMS of the spin packets with the largest shift of ±50 kHz exhibits the most intensive peaks at the half multiple of ($k\omega_{rf}$) or at position corresponding to $k = 1$, $k' = 2$ as defined in Eq. (4). Finally, contribution of all fifteen spin packets is summed up and cumulative DMS for the model of inhomogeneous line is shown in Fig. 7c. Here, one can clearly see the distribution of the most intensive peaks in the vicinity of multiple ($k\omega_{rf}$) and hence describes possible the origin of broadening in DMS. The obtained analyzes indicate that the additional broadening of DMS, besides saturation and modulation effects, can be produced by Ω_{SL} due to the influence of various distributions of B_L fields.

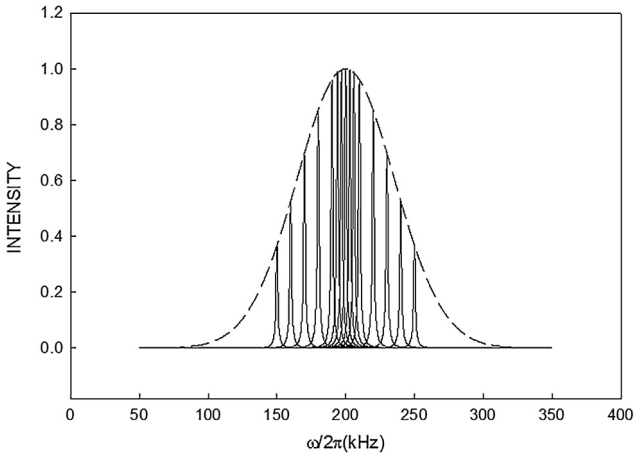

Fig. 6. Fifteen spin packets representing a simplified model for an inhomogeneous line. All spin packets are assumed to have the same linewidth of δ = 1.59 kHz. They are symmetrically positioned from the center of the spin packet: ten spin packets are mutually shifted by 10 kHz while four spin packets near the center by 2.5 kHz. Intensities of these spin packets are normalized using Gaussian line profile with $\Delta\nu_G$ = 83.25 kHz (dashed line).

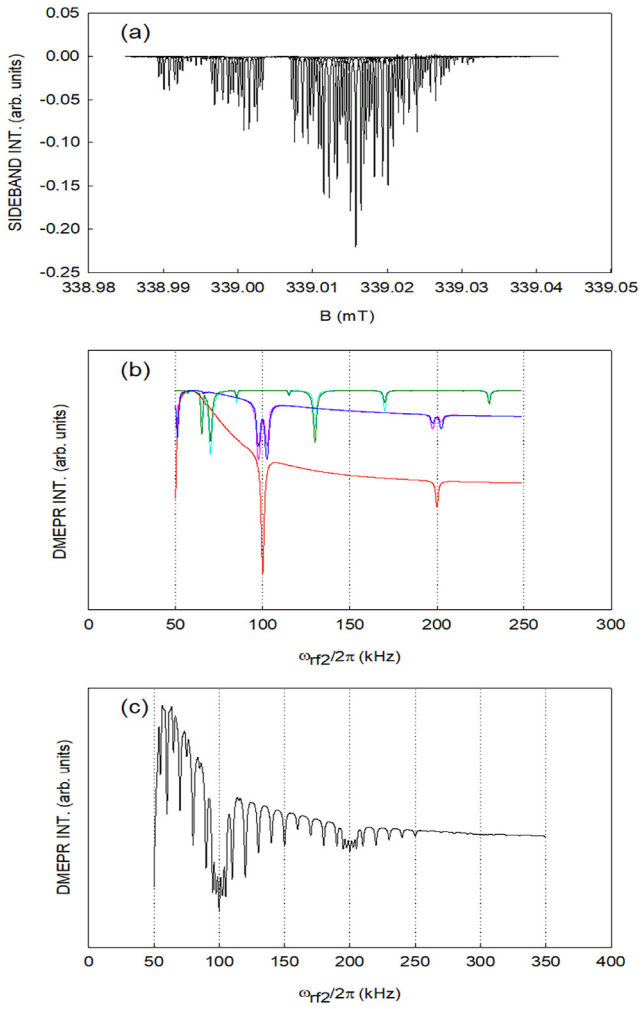

Fig. 7. Sideband (a) and double modulation (b, c) spectra of the inhomogeneous line described in Fig. 6. (a) The cumulative modulation sideband spectrum under the condition given in Fig. 3 of each spin packet in the inhomogeneous line presented in Fig. 6. Only the part of the antisymmetric spectrum with negative intensities is shown. (b) Some of the representative double modulation spectra obtained at B_{oos} for the largest modulation sideband intensity: at the center of the largest modulation sideband (a) (red line), at the spin packets shifted from the center spin packet by ±2.5 kHz (blue and pink lines) and at the sideband of spin packets shifted by ±50 kHz (cyan and green lines). Cumulative double modulation spectrum obtained from the sum of all double modulation spectra of the individual spin packets (c). (For interpretation of the references to colour in this figure legend, the reader is referred to the web version of this article.)

3. Detection of DM-EPR

3.1. Experimental

The CW-EPR, Pulsed-EPR and DM-EPR experiments were performed using a Bruker ELEXSYS 580 spectrometer working at X-band frequency accompanied with additional homemade RF modulation coil. The coil was inserted in the microwave cavity (rectangular TE_{102}) and oriented perpendicular to B_0 field in order to produce the second modulation in the cavity. The coil inserted in the cavity additionally decreases Q-value of the cavity and contributes to the lower intensity of MW field at the site of the sample than expected for the standard TE_{102} cavity. In order to avoid this inconvenience ω_1 was additionally controlled and estimated with MS method as discussed recently [17]. The RF source and the control of the modulation parameters were realized by employing continuous electron nuclear double resonance, ENDOR, module included in the spectrometer. Thus, DMS have been recorded in the same way and in the same format as ENDOR spectra at ELEXSYS spectrometer.

A well-known standard in CW-EPR spectroscopy E′-centers obtained by γ-irradiation (at dose of 1Mrad) of quartz tube (2 mm outer diameter) was used. Dependence of characteristic relaxation times T_1, T_2 and concentration of spins, C_S, on irradiated dose have been recently examined for this sample [18]. It is expected that for the applied radiation dose this sample exhibits $T_1 \approx T_2 = 200$ μs and C_S within interval of 10^{16}–10^{17} spins/cm^3.

The quartz sample employed in the present investigation was additionally characterized by applying Pulsed-EPR methods using the same spectrometer. Relaxation time $T_1 = 200$ μs was obtained by employing inversion recovery with spin echo-detection method while the phase memory time, $T_m = 43$ μs, ($T_m \leq T_2$) and $C_S \approx 2 \times 10^{17}$ spins/cm^3 were obtained in the process of extrapolation of the spin–echo intensity for small pulse turning angle $(\sin \theta)^2$.

3.2. DM-EPR spectra of E′ centers

DMS of E′ centers have been recorded and analyzed earlier in several studies [1,10,19–21]. The spectra were obtained by employing the first and the second harmonic detection. The obtained narrow lines at multiple of the first modulation frequency were significantly narrower (between two and three orders of magnitude) than the corresponding EPR linewidth. Besides that, underlying relaxation mechanism responsible for such sharp lines were not completely explained [1,8,10]. It is also noted, as mentioned above, that variations in the line shapes and corresponding linewidths of these lines arise due to small change of the employed spectroscopic parameters. Of course, these properties increase an uncertainty in assignation of underlying relaxation times. However, recently improved spectroscopic characterization of E′ centers [18,22] based on advanced spectroscopic methods resulted in higher accuracy of determined relaxation times T_1, T_2, and C_S than available in the previous studies. These parameters are essential in the calculation of MS spectrum of homogenous line as well as of the corresponding DMS in SFM regime in terms of multi-photon transitions. It is expected that DMS recorded for an inhomogeneous CW-EPR line of E′ centers by employing spectrometer parameters fined tuned to match SFM and WMRR modulation regimes will show spectra which could be scaled to spectra of homogeneous line.

In order to satisfy SFM and WMRR conditions by using standard arrangement of the first modulation frequency ($\omega_{rf}/2\pi = 100$ kHz) one needs to employ small amplitude of modulation ($\omega_2 < \omega_{rf}$). This condition gives low z value and results in a MS spectrum with low number of detectable sidebands. In Fig. 8 the small amplitude

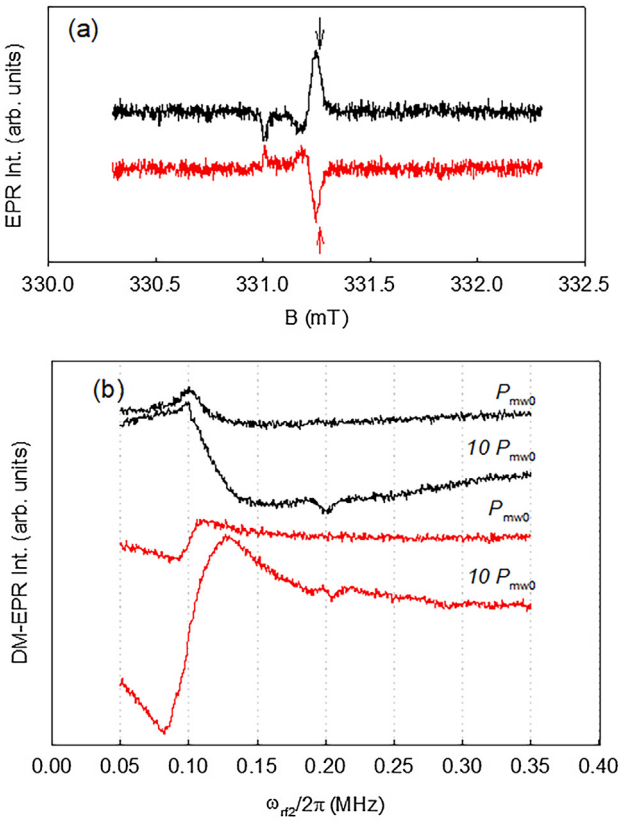

Fig. 8. (a) CW-EPR spectra of E′ center recorded in the strong and fast modulation regime of spin dynamics for two modulation phase angles, black spectrum at phase angle φ and red spectrum at phase angle φ + π/2. Spectra are recorded by employing parameters $\omega_{rf}/2\pi = 100$ kHz, $\omega_2/2\pi = 20$ kHz, and P_{mw0} ($P_{mw0} = 0.063$ mW corresponds to ($\omega_{10}/2\pi = 8.7$ kHz)). Arrows denote positions where double modulation spectra are obtained. (b) Double modulation spectra in the strong and fast modulation regime of spin dynamics obtained for modulation phase angle φ (black spectra) and for φ + π/2 (red spectra). Spectra are recorded by employing parameter $\omega_{22}/2\pi \sim 0.5$ MHz for two different microwave field intensities while other parameters are the same as given in Fig. 8a. (For interpretation of the references to colour in this figure legend, the reader is referred to the web version of this article.)

of modulation ($\omega_2/2\pi = 20$ kHz) was employed to detect DMS at two modulation phases (φ and φ + π/2). Detectable CW-EPR signal (Fig. 8a) for present experimental set-up at low intensity of microwave power ($P_{mw0} = 0.063$ mW) was employed to reach small amplitude of MW field ($B_{10} = 0.00062$ mT). The obtained DMS under the same conditions show only one peak (dispersion type of peak at 100 kHz) for both detection phases (Fig. 8b). By increasing ω_1 to higher values but still lower than an ω_{rf}, an additional sideband peak at 200 kHz can be noted in DMS. Fig. 8b shows example of DMS detected at $10P_{mw0}$ corresponding to $\omega_1/2\pi = 27$ kHz value. Again, the peak lineshapes of the first peaks (at 100 kHz) of these DMS at $10P_{mw0}$ indicate dominant dispersion over the absorption lineshape sideband contribution. Indeed, the multi-photon transitions calculation [12] predicts within order of magnitude larger dispersion contribution for the first sideband in MS detected at the first harmonic in the monitored modulation regime. Additionally, detected peaks at 200 kHz show dispersion-like lineshapes for the spectra detected at φ + π/2 phase and an absorption type of lineshapes for spectra detected at φ phase, respectively (Fig. 8b). The absorption peak exhibits composite character and can be better approximated with two Lorentzians than with only one average peak (Insert to Fig. 9a). Fitting parameters of the two Lorentzian shapes (amplitude intensities, I_1, I_2, linewidths, $\delta_1/2$, $\delta_2/2$ and peaks positions ω_{rf21}, ω_{rf22}) are plotted

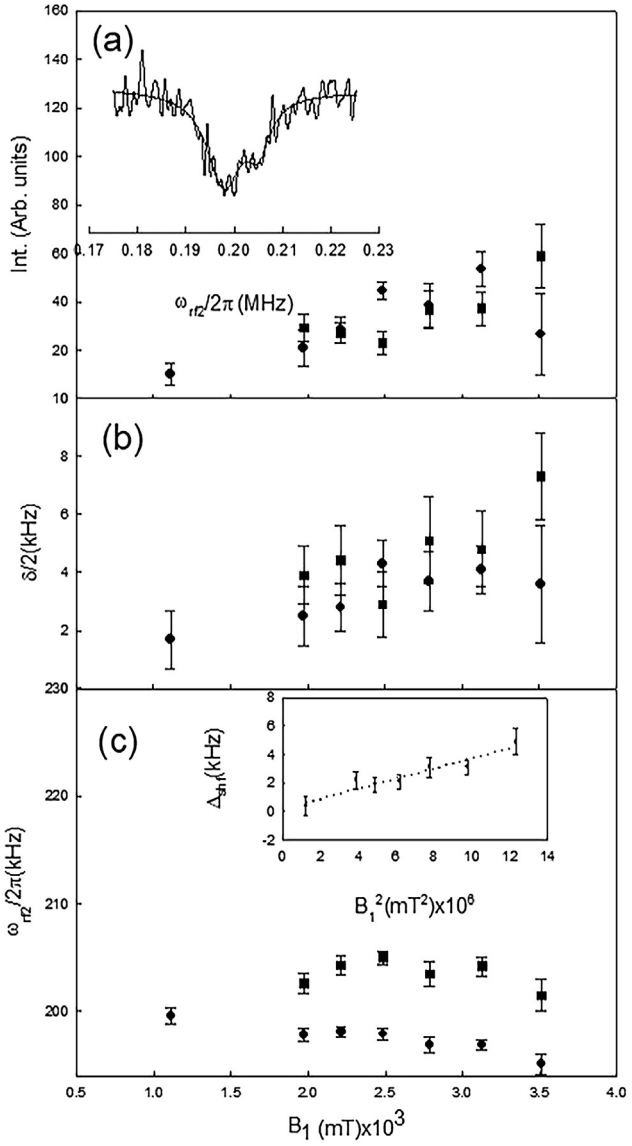

Fig. 9. Typical composite lineshape of double modulation peak detected at 200 kHz in the strong and fast modulation regime of spin dynamics were assumed two Lorentzian lineshapes (the cumulative fit is presented with continuous smooth line in the insert). Parameters of fitting: amplitude intensity I_1 (circles), I_2, (squares), linewidths $\delta_1/2$ (circles), $\delta_2/2$ (squares), and corresponding peak positions $\omega_{rf21}/2\pi$, (circles), $\omega_{rf22}/2\pi$ (squares) are shown from (a)–(c). The frequency shifts Δ_{shf} from 200 kHz to the low frequencies are plotted as a function of B_1^2 in the insert to (c). The dotted line describes linear behavior. Spectra are recorded by employing the same parameters as given in Fig. 8.

as a function of B_1 and collected in the three plots in Fig. 9a–c, respectively. It could be noticed that the sharper line δ_1 reached a value around 3 kHz when B_1 approached the zero value. This finding indicates an effective $T_2 \sim 110$ μs, which can be reached with DMS in the limit of small modulation amplitude and power saturation. It is interesting to note that by increasing P_{mw} the peak of the narrow line shifts to frequencies below the expected position at 200 kHz (Fig. 9c). On contrary, the peak of the second broader line ($\delta \sim 13$ kHz) shows opposite shift to frequencies above 200 kHz (Fig. 9c). The shift of sidebands due to MW saturation of MS was also theoretically predicted [12] in the form of $\Delta_{BS}(k)$ shift for both regimes of dynamics. The calculation shows that this effect significantly contributes only to the first and to the second sideband and, thus, it can be expected that only the low multiple frequency peaks of DMS will be affected with this shift. The possibility that contribution to DM-EPR peak originates from the sideband peaks from both sides of MS regarding the center of MS, one also expects contribution of such shift at the both sides of the peak. In the present case it can be noted in the Insert to the Fig. 9c that the peak shift of the narrow line Δ_{shf} shows linear behavior in the plot of Δ_{shf} *versus* B_1^2 and, hence, indicates expected shift [12,17] of the peak proportional to B_1^2 in the limit of small P_{mw}. This indicates possibility of the DM-EPR method to detect the effect of Bloch-Siegert-like shift within an inhomogeneous line. It can be also noted that the first sideband at 100 kHz shows broadening as well as significant shift of the peaks of dispersion lineshape on both sides regarding the center of dispersion lineshape. It is expected that this effect can be also qualitatively explained by considering the impact of the sideband dispersion line shift in MS [12] and the same argument as for DM-EPR absorption peak at 200 kHz under the P_{mw} saturation process. The above consideration was limited due to the small number of sidebands in MS and also due to the low signal to noise ratio since unusual small value of ω_2 for the standard detection of DMS of E' centers was applied. In order to improve the signal to noise ratio and to increase number of peaks for the given experimental parameters from the paragraph above, one can gradually increase only ω_2 parameter. Fig. 10 shows typical DMS obtained in the wide region of P_{mw} values by employing $\omega_2/2\pi = 0.6$ MHz. As in the case of small ω_2 detected peaks, here also the composite character of the lineshapes can be better approximated with two Lorentzian peaks than with one averaged Lorentzian (Insert to Fig. 10). In addition, Fig. 10 also shows an unexpected shape of DMS obtained in the high-power region. Surprisingly, composite peaks show saturation of broad components and significant increase in the amplitude of sharp components detected at high microwave power. The obtained sharp lines were examined in more detail in the high saturation region of P_{mw} by employing $B_{rf} = 0.1$ mT (Fig. 11). This modulation amplitude was chosen in order to easily correlate DMS with CW-EPR in-phase and out-of-phase saturation spectra of E' center which was studied earlier [18] at the same modulation amplitude. The composite peaks at $k\omega_{rf}/2\pi$ ($k = 2, 3,$,; 200 kHz, 300 kHz, 400 kHz and 500 kHz) in Fig. 11 can be fitted by employing two Lorentzian lineshapes. Typical Lorentzian parameters ($\delta/2$,

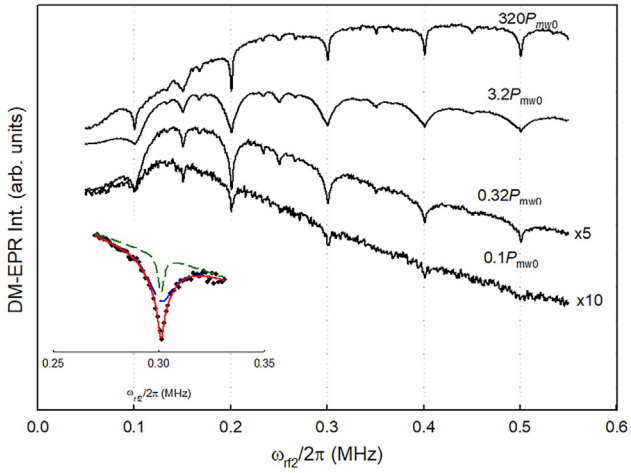

Fig. 10. Double modulation spectra of E′-centers detected in the wide range of spin dynamics ($\omega_2 > \omega_{rf}$, $\omega_2 > \omega_1$, from $\omega_1 \ll \omega_{rf}$ to $\omega_1 \gg \omega_{rf}$). Spectra are recorded by employing parameters $\omega_{rf}/2\pi = 100$ k Hz, $\omega_2/2\pi = 0.6$ MHz, $z = 24$, $\omega_{22}/2\pi \sim 0.5$ MHz for different P_{mw0}. The insert (filled circles) shows the enlarged peak at 300 kHz of the 0.32 P_{mw0} spectrum with fitted corresponding Lorentzian lineshapes, $\delta_1 = 3.2 \pm 0.8$ kHz (dashed, green) $\delta_2 = 15 \pm 3$ kHz (long dashed, blue) and cumulative line (continuous line, red). (For interpretation of the references to colour in this figure legend, the reader is referred to the web version of this article.)

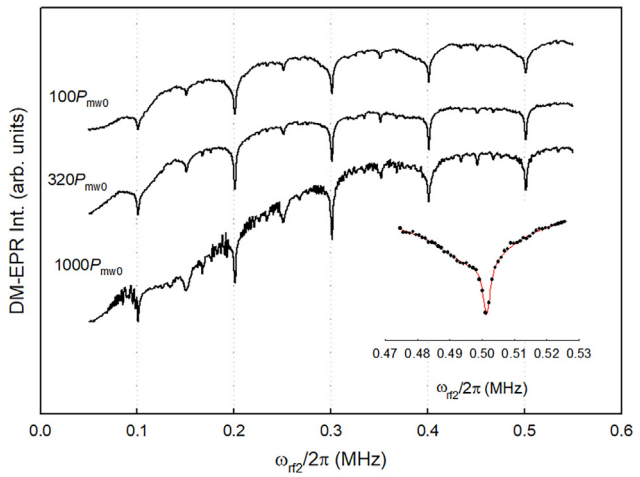

Fig. 11. Double modulation spectra of E′-centers detected at high microwave power region. Spectra are recorded by employing same parameters as given in Fig. 10 except for the $\omega_2/2\pi$ which was parameter increased to large value (1.4 MHz). The insert (filled circles) show the enlarged peak at 500 kHz of the third (at 100 P_{mw0}) spectrum with fitted cumulative line (full red line) of two corresponding Lorentzian lineshapes. (For interpretation of the references to colour in this figure legend, the reader is referred to the web version of this article.)

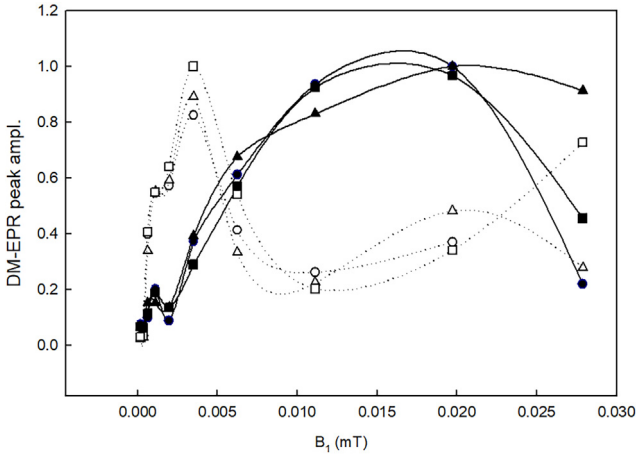

Fig. 13. Normalized amplitude with respect to the largest amplitude for the corresponding double modulation peak of two Lorentzian lineshapes obtained by fitting experimentally detected double modulation peaks at 200 kHz (circles), 300 kHz (triangles) and 500 kHz (squares), presented in Fig. 11, as a function of B_1. Full symbols denote amplitude of the narrow δ_1 line and empty symbols amplitude of the broad δ_2 line. The solid and dashed smoothed lines are used only to guide the eye.

I and peak position) obtained by fitting procedure for peak at 500 kHz as function of B_1 are shown in Figs. 12 and 13. It is easy to note that narrow and broad spectral components can be detected in the whole monitored interval of B_1 (Fig. 12). The narrow component exhibits well defined average linewidth $\delta_1 = 2.1 \pm 0.6$ kHz at peak position 501.5 ± 0.1 kHz and variable intensity which reaches maximum at high P_{mw} ($B_1 \sim 0.017$ mT). The broader component ($\delta_2 = 25.5 \pm 7.7$ kHz) shows larger variation of peak positions (500.1 ± 1.7 kHz) while the saturation appears at lower microwave power ($B_1 \sim 0.0035$mT) than for the sharp component. The peak with the smallest intensity at $B_1 \sim 0.0012$ mT can be clearly detected for all analyzed DM-EPR peaks for both components (Fig. 13). In addition, the comparison of DMS amplitude *versus* B_1 for the two components fitting the peaks at different multiple frequencies qualitatively show similar behavior and supports applied analyses.

Finally, it is also interesting to detect DMS at high z value. This can be easily achieved by increasing the amplitude or/and decreasing frequency of the first modulation frequency applied on the above detected spectra. Fig. 14 shows DMS of E′-centers detected at high z-values ($z = 14$, $z = 747$, $z = 1494$) with $\omega_{rf} = 30$ kHz. The spectra are presented for the same ω_{rf2} in the similar sweeping range as was used above for DMS obtained at $\omega_{rf} = 100$ kHz. It can be noted that significantly large number of peaks with mutual distances of 30 kHz in the monitored interval appears. The narrowest peaks ($\delta \sim 3$ kHz) appear at spectrum with the largest z value as illustrated in the Insert to Fig. 14.

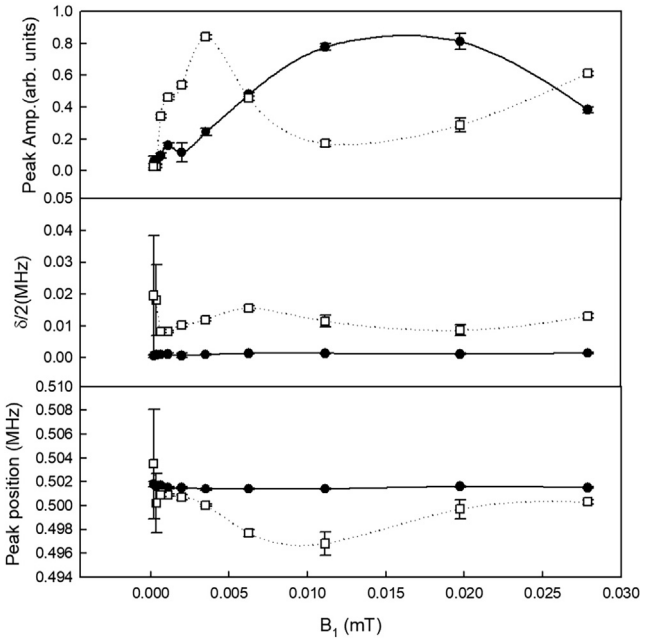

Fig. 12. Parameters of two Lorentzian lineshapes obtained by fitting experimentally detected peak at 500 kHz of double modulation spectra presented in Fig. 11 as a function B_1. The parameters for narrower Lorentzian lineshape, peak amplitude, half of linewidth, and peak position are denoted with filled circles and parameters for broader Lorentzian lineshape with open squares. The solid and dashed smoothed lines are used only to guide the eye.

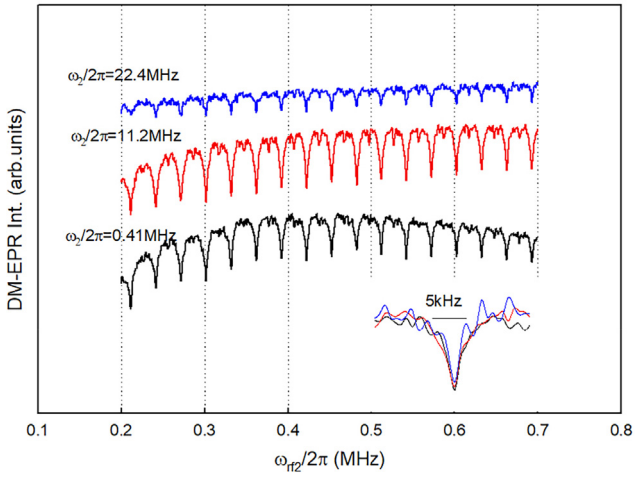

Fig. 14. Double modulation spectra of E′-centers detected at the first modulation frequency $\omega_{rf} = 30$ kHz. Spectra are recorded by employing parameters $P_{mw} = 10$ P_{mw0} and $\omega_{22}/2\pi \sim 0.5$ MHz for different modulation amplitudes. The insert shows the enlarged and normalized peaks for all three double modulation spectra at the same multiple $k = 20$ of the first modulation frequency (600 kHz).

4. Discussion

Beside the composite character of the peaks, over-all shapes of the entire experimentally detected DMS of an inhomogeneous line in the limit of low P_{mw} show high similarity to spectra of homogeneous line and could be easily scaled with the calculated model in order to evaluate effective relaxation times (T_1, T_2). DMS (Fig. 8) detected in the limit of weak microwave power ($\omega_1/2\pi \approx 3$ kHz) shows that the narrow component of the linewidth is more pronounced in comparison to the broader one and can be correlated with the homogeneous line model spectrum calculated for nearly the same microwave power saturation ($\omega_1/2\pi = 5.5$ kHz), as shown in Fg.4. It is also interesting to note that the model spectrum exhibits broadening of calculated modulation peaks with $\delta = 6.07$ kHz and $\delta = 3.28$ kHz due to the saturation effects and resonance position of B_{oos}, respectively. This indicates possibility that the lowest P_{mw} applied in the above experiment already contributes to the broadening of the peaks in DMS. Thus, a new setup of the experiment is required with improved signal-to-noise ratio to check δ at P_{mw} lower than the lowest P_{mw} in the present experiment.

The above considerations show that description of MS which is based on the multi-photon transitions for SFM dynamics regime also describes DMS in the limit of low P_{mw}. This theoretical model of DMS supports the finding that linewidths of detected narrow peaks originate from T_2-type of spin relaxation. In the WMRR spin dynamics regime, which is obtained by further increasing P_{mw} until ω_1 reaches the value of ω_{rf} (or $2\omega_{rf}$), MS spectrum can be further analytically described and also applied to describe DM-EPR spectra similarly as for SFM regime. It should be noted that an analytical calculation of MS was here provided only for regime of weak resonance modulation ($\omega_2 \ll \omega_1 \approx \omega_{rf}$) while in the regime of strong resonance modulation ($\omega_2 \gg \omega_1 \approx \omega_{rf}$) such model is missing since the same calculation methodology could not be applied [12]. However, for the sample containing centers with long relaxation times this type of regime usually coincides with the well known "rapid passage" regime for EPR signal [15,16]. It appears when the rate of change of ω_2 (or B_0) is faster than the electron spin relaxation time. Recently, the "rapid passage" effect for E′ centers in quartz was studied in CW-EPR by employing modulation frequency of 100 kHz [18,22]. Theoretical description of the obtained amplitude of EPR signal, in-phase and out-of-phase with respect to the modulation frequency, was calculated by employing numerical solution of Bloch equations. Moreover, in the study [18] amplitude and phase behavior of the signal was provided from low-power to high-power range of microwave intensities. It is assumed that, as B_1 increased the effective T_2 required to match the experimental signal intensity increased, as well at high B_1 ($B_1 > 0.01$ mT) the effective T_2 became equal to T_1. Thus, one expects that spectral lines in MS as well as lines in DMS would also show similar enhancement behavior for "rapid passage" regime under microwave saturation.

It is interesting to note that detected 100 kHz component in Fourier transforms of the waveforms for the E′ signal in CW-EPR experiment [18], obtained at 0.1 mT modulation amplitude as a function of B_1, shows similar behavior as amplitude of DM-EPR peaks. Amplitude of Fourier transform (Ref. [18], Fig. 5) exhibits two maxima, the first (with intensity ~1/3 of the second maximum) appears at $B_1 \approx 0.002$ mT and the second at $B_1 \approx 0.025$ mT, respectively. Thus, the shape and extremes of amplitude dependence vs. B_1 for EPR Fourier transform components and DM-EPR peaks can be scaled and qualitatively discussed in terms of the relaxation phenomena involved in this process. The amplitude of narrow component of DM-EPR peak (Fig. 12) as a function of B_1 indeed exhibits very similar behavior as amplitude of Fourier transform component in (Ref. [18], Fig. 5) by showing two maxima. The maximum at higher B_1 can be employed to define an enhancement for the rapid passage regime as the ratio between in-phase EPR signal amplitude at low B_1 and out-of-phase EPR signal at high B_1, respectively. For the 1 Mrad-sample this EPR signal ratio is expected ~9 [18] and for DM-EPR for narrow peak amplitudes ~15, respectively. For the EPR experiment the effective T_2 was estimated in the process of scaling of the functional dependence, amplitude vs. B_1, by assuming that effective T_2 is equal to T_2 at maximum amplitude in the region of high B_1. On the other side, for DM-EPR case, the obtained linewidth of the narrow component directly represents an effective $T_2 = 152 \pm 43$ μs for entire monitored B_1 interval with value of $T_2 \approx 145$ μs at the maximum value (Fig. 12). It is interesting to note that the obtained T_2 values satisfied the condition $T_2 \leq T_1$ within the experimental error for expected $T_1 = 200$ μs. The maximum of DM-EPR amplitude for second peak δ_2 at 500 kHz appeared at significantly lower $B_1 \approx 0.0035$ mT than the maximum of δ_1. In addition, a larger variation of δ_2 in linewidths and peak positions during saturation procedure indicates more inhomogeneous character of δ_2 components in comparison to δ_1 peak components. The obtained corresponding effective $T_2 = 12.5 \pm 3.7$ μs for this peak component was not detected for the amplitude of Fourier transform of CW-EPR experiment in (Ref. [18], Fig. 5) and could not be simply assigned as was assigned δ_1 peak.

The contribution of a "rapid passage" on DMS was not recognized in the previous studies of DM-EPR experiments. This finding can open a new possibility in interpretation of DMS spectra. For example, DMS obtained in irradiated alanine [7] was detected under high P_{mw} and the correlation with the effective T_2 could be more reliably assigned by employing additional arguments related to "rapid passage" effect. It is also known that "rapid passage" effect can be apply to enhance detection signal in CW-EPR as well as DM-EPR and it is more convenient in detection of low concentration of paramagnetic centers in comparison to Pulsed EPR [22]. Indeed, our preliminary DMS of low concentration NV centers in diamond under the high power saturation exhibits DMS with sharp peaks in the range of expected T_2 values for this center. On the other side the same results could not be obtained by applying Pulsed EPR due to lack of echo signal detection for the same sample (work in progress).

At this moment, it is also interesting to examine possible effect of Rabi resonance on DM-EPR spectrum. On the plot of DMS peak amplitude vs B_1 for each δ_1 and δ_2 lines at $B_1 \approx 0.0012$ mT (Fig. 12) the first peak which can be noted coincides with the first peak of the amplitude of Fourier transform [18]. The following minimum near this peak was assigned [12] to an effect of Rabi resonance on MS spectrum. Thus, it is expected that the same effect can be involved in DM-EPR peak intensity. Fig. 13 shows well defined position of the minima at $B_1 \approx 0.0018$ mT in the plot of amplitude vs B_1 for both components of peak for several DM-EPR multiple peaks.

DMS with high z-value for an inhomogeneous line shows qualitatively similar behavior as was predicted for calculated DMS of the homogeneous line. For the E' center the sharp peaks appear at high z-values approaching δ expected for homogeneous line of this center. It is important to note that again some of the peaks in Fig. 14 could be also approximated with two components (δ_1 and δ_2) as was discussed for spectra at $\omega_{rf} = 100$ kHz. Of course, here one expects that δ_1 component will be similar to δ_1 component obtained at $\omega_{rf} = 100$ kHz. However, an average δ_2 component estimated at $\omega_{rf} = 30$ kHz peaks will be significantly narrower than the average δ_2 component obtained at $\omega_{rf} = 100$ kHz. These evidences that δ_2 line component depends more

on applied experimental parameters than the δ_1 line component δ_2 can be generally correlated with T_m-type ($\delta_2 = 1/\pi T_m$) values usually obtained in pulsed-EPR experiments. Additionally, due to slower modulation rate at 30 kHz than at 100 kHz it is expected that the effect of "rapid passage" under saturation of DMS is reduced at lower frequencies.

Finally, the above considerations give new evidences to correctly decided between two different suggestions about the origin of DMS peaks. As shown above for the low P_{mw} discussed multi-photon transitions model of DMS peaks originated from the T_2 relaxation mechanism. The earlier evidence that DMS peaks of E' centers were due to T_1 relaxation mechanism [19] can be also reinterpreted by assuming that T_2 relaxation mechanism is involved through the effective T_2 relaxation which has the value equal to T_1 in the regime of "rapid passage" detection at high P_{mw}.

5. Conclusion

As shown above the DMS can be treated as one specific type of MS which can be produced from an ordinary homogeneous line. Theoretical description of this MS in the low saturation limit was given in terms of multi-photon transitions, which include MW photon in combination with arbitrary number of RF photons. Moreover, similar specific type of MS also appears within an inhomogeneous line and can be deduced by applying DM-EPR methodology. This property enables to detect narrow lines from the broader inhomogeneous lines and hence provide more information on the nature of inhomogeneity of the monitored line.

It is important to note that effects of larger intensity of dispersion than absorption shape of sidebands in DMS and splitting of absorption lineshape of sideband detected for the second absorption sideband in Fig. 9 can be explained only within the recent model of the multi-photon MW and RF transitions.

The presented study of inhomogeneous CW-EPR line of E' centers in quartz demonstrate capability of the method in comparison with other advanced EPR methods (Pulsed-EPR, "rapid passage" detection CW-EPR) to deduce homogeneous lines from this center. The obtained results support DM-EPR method as an additional complementary method for studying inhomogeneous broadening in the EPR spectra.

Acknowledgment

This work was supported in part by the Croatian Science Foundation under the project number IP-2018-01-3168.

References:

[1] B. Rakvin, T. Islam, I. Miyagawa, Modulation spectrum from an electron-spin-resonance line, Phys. Rev. Lett. 50 (1983) 1313–1315.
[2] B. Rakvin, Detection of very slow motions of nitroxide spin labels from double modulation electron-spin-resonance spectra, Chem. Phys. Lett. 109 (1984) 280–284.
[3] M. Peric, B. Rakvin, A. Dulcic, Double modulation techniques in electron-spin-resonance and slow rotations of nitroxide spin labels, J. Chem. Phys. 82 (1985) 1079–1084.
[4] M. Peric, B. Rakvin, A. Dulcic, Hindered rotation of methylene groups in irradiated zinc acetate dihydrate – a double modulation electron-spin-resonance study, Chem. Phys. Lett. 126 (1986) 574–578.
[5] S. Valic, B. Rakvin, Z. Veksli, Z. Grubisicgallot, Study of slow molecular-motion of spin probes in polymers by the double-modulation Esr method, Macromolecules 23 (1990) 5182–5186.
[6] B. Rakvin, Sensitivity of the method of double-modulation Esr detection of electron spin-lattice relaxation-time, J. Magn. Reson. Ser. A 106 (1994) 245–247.
[7] B. Rakvin, Double modulation ESR study of irradiated alanine, Appl. Radiat. Isotopes 47 (1996) 1251–1255.
[8] A. Dulčić, M. Perić, Theory of double-modulation spectra in inhomogeneously broadened lines, J. Magnet. Reson. 76 (1988) (1969) 427–439.
[9] O. Haworth, R.E. Richards, The use of modulation in magnetic resonance, Progr. Nucl. Magnet. Reson. Spectrosc. 1 (1966) 1–14.
[10] M. Giordano, D. Leporini, M. Martinelli, L. Pardi, S. Santucci, C. Umeton, Double-modulation electron-spin-resonance spectroscopy: experimental observations and theoretical comprehensive interpretation, Phys. Rev. A 38 (1988) 1931–1942.
[11] M. Kalin, I. Gromov, A. Schweiger, The continuous wave electron paramagnetic resonance experiment revisited, J. Magnet. Reson. 160 (2003) 166–182.
[12] A.P. Saiko, R. Fedaruk, S.A. Markevich, Multi-photon transitions and Rabi resonance in continuous wave EPR, J. Magnet. Reson. 259 (2015) 47–55.
[13] M. Kälin, M. Fedin, I. Gromov, A. Schweiger, Multiple-photon transitions in EPR spectroscopy, in: J. Dolinšek, M. Vilfan, S. Žumer (Eds.), Novel NMR and EPR Techniques, Springer, Berlin Heidelberg, Berlin, Heidelberg, 2006, pp. 143–183.
[14] A.P. Saiko, G.G. Fedoruk, S.A. Markevich, Multiphoton transitions in a spin system driven by strong bichromatic field, J. Exp. Theor. Phys. 105 (2007) 893–899.
[15] A.M. Portis, Rapid passage effects in electron spin resonance, Phys. Rev. 100 (1955) 1219–1221.
[16] M. Weger, Passage effects in paramagnetic resonance experiments, The Bell System Tech. J. 39 (1960) 1013–1112.
[17] B. Rakvin, D. Carić, M. Kveder, Enhanced accuracy of the microwave field strength measurement in a CW-EPR by pulsed modulation technique, J. Magnet. Reson. 287 (2018) 123–127.
[18] J.R. Harbridge, G.A. Rinard, R.W. Quine, S.S. Eaton, G.R. Eaton, Enhanced signal intensities obtained by out-of-phase rapid-passage EPR for samples with long electron spin relaxation times, J. Magnet. Reson. 156 (2002) 41–51.
[19] P.G. Belov, A.D. Milov, Double-modulation ESR and electron spin echo study of paramagnetic centres in fused quartz: comparison of techniques, Chem. Phys. Lett. 151 (1988) 79–82.
[20] I. Miyagawa, G. Iyer, F.B. Majid, Linewidth of the ESR modulation spectrum, Chem. Phys. Lett. 175 (1990) 441–444.
[21] F.B. Majid, I. Miyagawa, Detection of several types of the E′ center by the ESR double-modulation spectrum method, Chem. Phys. Lett. 209 (1993) 469–473.
[22] D.G. Mitchell, R.W. Quine, M. Tseitlin, V. Meyer, S.S. Eaton, G.R. Eaton, Comparison of continuous wave, spin echo, and rapid scan EPR of irradiated fused quartz, Radiat. Meas. 46 (2011) 993–996.